materials

MDPI

Article

Effect of SO_2 on the Selective Catalytic Reduction of NO_x over V_2O_5-CeO_2/TiO_2-ZrO_2 Catalysts

Yaping Zhang [1], Peng Wu [1], Ke Zhuang [2], Kai Shen [1,*], Sheng Wang [2,*] and Wanqiu Guo [1]

[1] Key Laboratory of Energy Thermal Conversion and Control of Ministry of Education, School of Energy and Environment, Southeast University, Nanjing 210096, China
[2] State Power Environmental Protection Research Institute, Nanjing 210031, China
* Correspondence: shenkai@seu.edu.cn (K.S.); wpp67890@163.com (S.W.); Tel.: +025-83790667 (K.S.)

Received: 23 June 2019; Accepted: 5 August 2019; Published: 9 August 2019

Abstract: The effect of SO_2 on the selective catalytic reduction of NO_x by NH_3 over V_2O_5-0.2CeO_2/TiO_2-ZrO_2 catalysts was studied through catalytic activity tests and various characterization methods, like Brunner–Emmet–Teller (BET) surface measurement, X-ray diffraction (XRD), transmission electron microscopy (TEM), X-ray fluorescence (XRF), hydrogen temperature-programmed desorption (H_2-TPR), X-ray photoelectron spectroscopy (XPS) and in situ diffused reflectance infrared Fourier transform spectroscopy (DRIFTS). The results showed that the catalyst exhibited superior SO_2 resistance when the volume fraction of SO_2 was below 0.02%. As the SO_2 concentration further increased, the NO_x conversion exhibited some degree of decline but could restore to the original level when stopping feeding SO_2. The deactivation of the catalyst caused by water in the flue gas was reversible. However, when 10% H_2O was introduced together with 0.06% SO_2, the NO_x conversion was rapidly reduced and became unrecoverable. Characterizations indicated that the specific surface area of the deactivated catalyst was significantly reduced and the redox ability was weakened, which was highly responsible for the decrease of the catalytic activity. XPS results showed that more Ce^{3+} was generated in the case of reacting with SO_2. In situ DRIFTS results confirmed that the adsorption capacity of SO_2 was enhanced obviously in the presence of O_2, while the SO_2 considerably refrained the adsorption of NH_3. The adsorption of NO_x was strengthened by SO_2 to some extent. In addition, NH_3 adsorption was improved after pre-adsorbed by SO_2 + O_2, indicating that the Ce^{3+} and more oxygen vacancy were produced.

Keywords: V_2O_5-CeO_2/TiO_2-ZrO_2; selective catalyst reduction; catalyst; in situ DRIFTS; SO_2

1. Introduction

Selective catalytic reduction (SCR) catalysts are commonly severely deactivated by SO_2, which is abundantly present in flue gas. There are two mechanisms that can explain the sulfur poisoning of catalysts. Firstly, SO_2 reacts with NH_3 and vapor in the oxygen atmosphere, producing sulfate species including ammonium sulfate and ammonium bisulfate. These sulfate substances can deposit on the catalytic surface and cause pore plugging. As a result, the specific surface area and pore volume decrease observably, ending up with the catalyst deactivation. Studies have shown that the thermal decomposition temperature range of ammonium sulfate and ammonium bisulfate are 213–308 °C and 308–419 °C [1], respectively. It is still hard for these sulfate species to decompose over a traditional V/TiO_2 catalyst. In the second, SO_2 can react with the active center atoms and produce metal sulfates, which will decrease catalyst activity [2,3]. The former deactivation is reversible and the catalysts can be reactivated by washing and high-temperature processing. However, the later deactivation is irreversible.

The mechanism of catalyst sulfur poisoning has been extensively studied. Wei et al. [4] claimed that SO_2 significantly reduced the adsorption of NH_3 on the Lewis acid sites. At the same time, SO_2

would react with NH_4^+ to form NH_4HSO_3, thereby reducing NO_x conversion. However, Jiang et al. [5] proposed that SO_2 had little effect on the adsorption of NH_3, and conversely promoted the formation of new Bronsted acid sites. The weakening of NO adsorption on the catalyst surface was the main cause of deactivation. With the deposition of sulfate on the catalyst surface, less NO participated in the SCR reaction, resulting in a decrease in NO_x conversion. Similarly, Liu et al. [6] claimed that SO_2 had a significant inhibitory effect on the reduction of NO_x due to the deposition of sulfate substances. It hindered the adsorption of NO and the production of the intermediate ammonium nitrate, resulting in a decrease in catalyst activity. Moreover, Pan et al. [7] found that the main reason for MnO_x/TiO_2 catalysts deactivation was that the active center atom manganese was sulfated. Besides, the presence of SO_2 caused ammonium sulfate to deposit on the catalyst, decreasing the adsorption of NO. Gu et al. [8] reported that the main reason for the deactivation of Ce/TiO_2 catalyst was that SO_2 could react with the catalyst to form high thermally stable $Ce(SO_4)_2$ and $Ce_2(SO_4)_3$, and Xu et al. obtained similar results [9].

On the basis of the above literatures, it is found that there are still many controversies about the mechanism of catalyst sulfur poisoning. Moreover, there is no report found currently on the sulfur poisoning mechanism of V_2O_5-CeO_2/TiO_2-ZrO_2 catalysts, which were reported to be an excellent SCR catalyst with a wide temperature range [10–12]. Our previous studies indicated that the V_2O_5-$0.2CeO_2/TiO_2$-ZrO_2 catalyst exhibited superior catalytic performance as well as high tolerance of SO_2 and H_2O.In this paper, the catalytic activity of V_2O_5-$0.2CeO_2/TiO_2$-ZrO_2 in the presence of different SO_2 content was further studied. Various characterization methods such as the Brunner−Emmet−Teller (BET) surface measurement, X-ray diffraction (XRD), transmission electron microscopy (TEM), X-ray fluorescence (XRF), hydrogen temperature-programmed desorption (H_2-TPR), X-ray photoelectron spectroscopy (XPS) and in situ diffused reflectance infrared Fourier transform spectroscopy (DRIFTS) were employed to study the poisoning mechanism from a microcosmic aspect.

2. Materials and Methods

2.1. Catalyst Preparation

The Ti–Zr carrier was prepared by a coprecipitation method with the molar ratio of Ti:Zr = 1:1. An equal amount of $TiCl_4$ solution and $ZrOCl_2$ $8H_2O$ were dissolved in deionized water and stirred constantly. With stirring, $NH_3{\cdot}H_2O$ was slowly added until the pH reached 10. The obtained solution was aged at room temperature for 24 h. Then, the precipitate was washed with deionized water until the supernatant contained no Cl^-. Finally, the sample was dried at 110 °C for 12 h and then calcined at 450 °C for 4 h in a muffle furnace.

A step-by-step impregnation method was used to prepare V_2O_5-$0.2CeO_2/TiO_2$–ZrO_2. A certain amount of $CeNO_3{\cdot}6H_2O$ and Ti–Zr powder were added to deionized water. The obtained suspension was stirred at room temperature for 2 h, followed by stirred at 85 °C for 4 h. After dried at 110 °C for 12 h and calcined in a muffle furnace at 450 °C for 4 h, the Ce/Ti–Zr sample was obtained. Thereafter, the resulting Ce/Ti–Zr was impregnated with NH_4VO_3 solution in the same manner. The obtained sample was denoted as V-0.2Ce/Ti–Zr, where the content of V_2O_5 loading was 1 wt. % and the molar ratio of Ce to Ti–Zr support = 0.2.

For short, the V-0.2Ce/Ti–Zr catalyst after reaction with 0.06% SO_2 for 2 h was denoted as S-V-0.2Ce/Ti–Zr, while the catalyst after reaction with 10 vol% H_2O and 0.06% SO_2 for 2 h was denoted as HS-V-0.2Ce/Ti–Zr, respectively.

2.2. Activity Measurements

The SCR activity measurement of catalysts was carried out in a fixed-bed reactor with the inner diameter of 7 mm. The 0.3 g catalyst (40–60 mesh) was placed in the reactor with a gas hourly space velocity (GHSV) of 20000 h^{-1}. Typically, the total gas flow was 100 mL/ min. The simulated gas was composed of 0.08% NO, 0.08% NH_3, 5% O_2, 5%/10% H_2O (when used), 0.02%/0.04%/0.06% SO_2 (when

used) and N_2 as the balanced gas. The NO, NO_2 and NO_x concentration were persistently monitored with a flue gas analyzer (Testo350-XL).

2.3. Catalyst Characterization

The BET was measured using a specific surface area and pore size analyzer V-Sorb 2800P (Beijing Gold APP, Beijing, China). The sample was pretreated under vacuum at 250 °C for 5 h, and the adsorbate was high purity nitrogen.

XRD patterns were carried out for phase analysis via a SmartLab™ X-ray diffractometer (Rigaku, Tokyo, Japan). Cu target acted as the X-ray source.

The morphology of the catalyst was determined by TEM (Thermo Fisher Scientific, Waltham, Massachusetts, America). The catalyst sample was dispersed in an ethanol solution after thoroughly ground, followed by shaken under ultrasonic waves for 15 min.

XRF spectrometer (Thermo Fisher Scientific, Waltham, Massachusetts, MA, America) was used to analyze the content of component in the catalyst sample.

H_2-TPR was carried out in a quartz U-tube reactor connected to a thermal conduction detector (TCD) using an H_2–Ar mixture (10% H_2 by volume) as reductant (Finetec Instruments, Hangzhou, Zhejiang, China). The temperature range during the test was for 25 °C to 800 °C with a heating rate of 10 °C /min.

XPS analysis was performed on a PHI Quantera II system (Ulvac-PHI, Chigasaki, Kanagawa Prefecture, Japan). The binding energies were referenced to the C 1 s line at 284.8 eV from adventitious carbon.

In situ DRIFTS studies were performed on a Nicolet 6700 spectrometer (Thermo Fisher Scientific, Waltham, Massachusetts, MA, USA). The scanning wave number ranged from 400 cm^{-1} to 4000 cm^{-1}. Before the test, the sample was pretreated with N_2 at 400 °C for 1 h to remove impurities. The background at a certain temperature was collected during the cooling process.

3. Results and Discussion

3.1. Effects of SO_2 and H_2O on Catalyst Activity

Figure 1 showed the catalytic activity results with different concentration SO_2 over the V-0.2Ce/Ti–Zr catalyst at 250 °C. In the absence of SO_2, NO_x conversion of the V-0.2Ce/Ti–Zr catalyst was approximately 90%, indicating that the catalyst had high activity at the low temperature. After 0.02% SO_2 was introduced, NO_x conversion remained stable. However, NO_x conversion decreased rapidly to 71% and 65% at 20 min respectively when 0.04% and 0.06% SO_2 were added. Furthermore, it could be found that the catalytic activity could recover after stopping SO_2. It was inferred that SO_2 and SO_3 reacted with NH_3 in the early stage, leading to the decrease of NH_3 as well as the catalytic performance. As the reaction went on, SO_2 and SO_3 reacted with CeO_2 and produced Ce^{3+} in the presence of excess oxygen, which could strengthen the acid sites on the catalyst and increased NO_x conversion [13].

The effect of H_2O on the catalytic activity of the catalyst was investigated and the results were shown in Figure 2. It was found that the activity of the catalyst was rapidly decreased with the introduction of H_2O. However, after the H_2O was stopped, the activity gradually recovered almost to the original level, thus indicating that the effect of H_2O on the catalyst was reversible.

The activity of the V-0.2Ce/Ti–Zr catalyst was tested at 250 °C in the presence of 10% H_2O and different concentrations of SO_2, and the results were shown in Figure 3. After the introduction of SO_2 and H_2O, NO_x conversion decreased rapidly to less than 30%, which was much lower than that in the presence of SO_2 or H_2O alone. After SO_2 and H_2O were removed, NO_x conversion increased to some extent but could not be restored to the initial level, indicating an irreversible deactivation occurred. Studies showed that SO_2 would react with NH_3 to form ammonium sulfates, and block active sites on the surface of the catalyst.

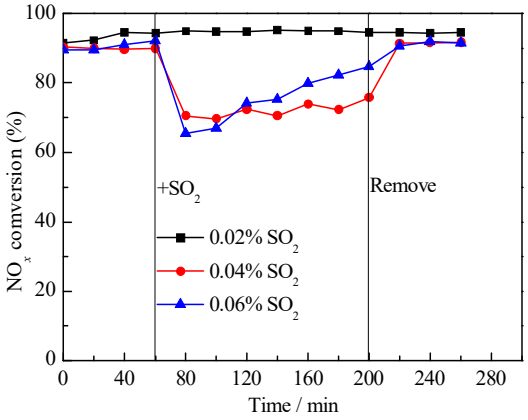

Figure 1. NO_x conversion of V-0.2Ce/Ti–Zr in the presence of SO_2 (250 °C). Reaction condition: NH_3 = NO = 0.08%, O_2 = 5%, N_2 as balance, SO_2 content: 0.02%, 0.04% and 0.06%, all by volume).

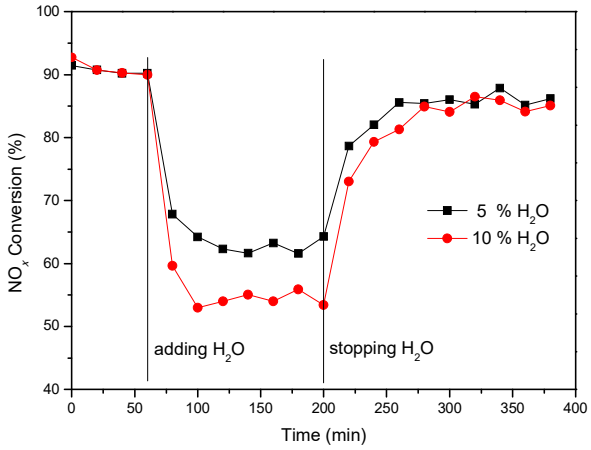

Figure 2. NO_x conversion of V-0.2Ce/Ti–Zr in the presence of H_2O (250 °C).

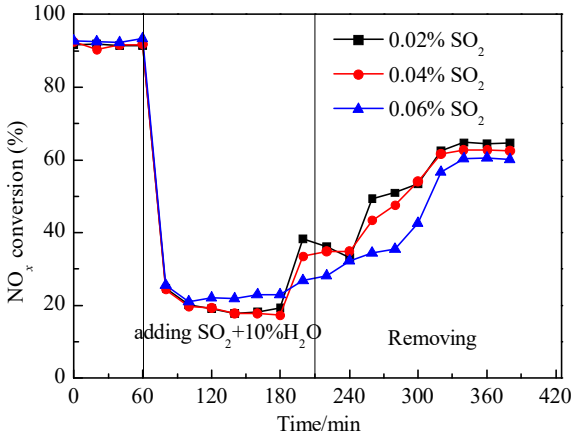

Figure 3. NO_x conversion of V-0.2Ce/Ti–Zr in the presence of H_2O and SO_2 (250 °C; reaction condition: NH_3 = NO = 0.08%, O_2 = 5%, H_2O = 10%, SO_2 = 0.02%, 0.04% and 0.06%, all by volume.

Furthermore, the performance of the HS-V-0.2Ce/Ti–Zr catalyst at different temperatures was also tested, and the results were shown in Figure 4. It could be found that the mid-temperature (200–300 °C) activity of the HS-V-0.2Ce/Ti–Zr catalyst was significantly decreased, while it at a higher temperature (>300 °C) was obviously enhanced. One literature indicated that the formation of $Ce(SO_4)_2$ led to a

decrease in the activity of the catalyst at moderate temperatures [14]. At the same time, Xu et al. [15] pointed out that the sulphate was produced during the poisoning process, which had a certain activity at high temperatures and could improve the high temperature activity of the catalyst.

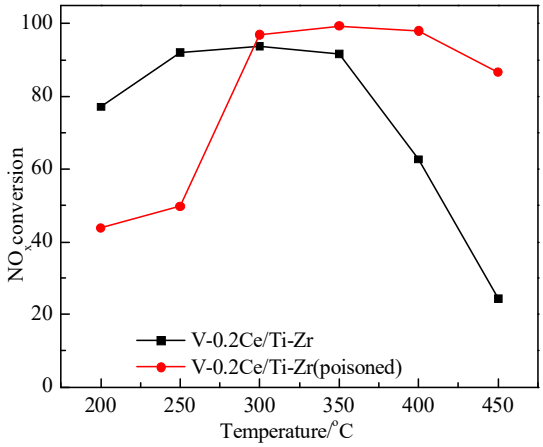

Figure 4. NO_x conversion of the V-0.2Ce/Ti–Zr and HS-V-0.2Ce/Ti–Zr catalyst.

3.2. Physico-Chemical Characterization of Catalysts

3.2.1. BET Analysis

The specific surface area of the catalysts before and after being poisoned by SO_2 was illustrated in Table 1. Compared with the fresh sample, the BET surface area of the S-V-0.2Ce/Ti–Zr catalyst decreased from 54.45 m^2/g to 25.07 m^2/g, and that of the HS-V-0.2Ce/Ti–Zr catalyst further reduced to 15.27 m^2/g. While with comparison to the fresh counterpart, there was no apparent change on the pore volume. The specific surface area of the catalyst was related to the adsorption capacity of NH_3 during the SCR reaction, thereby further affecting the denitrification activity.

Table 1. BET surface area and pore volume of the fresh and poisoned catalyst.

Sample	BET Surface Area (m^2/g)	Pore Volume (mL/g)
V-0.2Ce/Ti–Zr	54.45	0.14
S-V-0.2Ce/Ti–Zr	25.07	0.16
HS-V-0.2Ce/Ti–Zr	15.27	0.11

In order to further investigate the reason for the significant decrease in the BET specific surface area, the pore size distribution of the catalyst was mapped. As shown in Figure 5, the pore size range of the fresh catalyst was mainly concentrated at 2 nm to 10 nm, indicating that the mesopores contributed the most to the specific surface area of the catalyst. For the catalyst after reaction with O_2, the number of macropores and mesopores (in the range of 5.3 nm to 50 nm) increased, and the increase of pore diameter in HS- V-0.2Ce/Ti–Zr catalyst was more pronounced. It was found that the mesopores (mainly 2 nm to 10 nm) contributed the most to the specific surface area of the catalyst. Therefore, it was presumed that the number of mesopores determined the NH_3-SCR activity of the V-0.2Ce/Ti–Zr catalyst. After the reaction in presence of H_2O and SO_2, mesopores in the range of 5–50 nm contributed greatly to the specific surface area of the catalyst, while the mesopores and micropores with pore diameters less than 5 nm gradually decreased. Based on the above analysis, it was speculated that in the presence of SO_2 and H_2O, $(NH_4)_2SO_4$ and $Ce(SO_4)_2$ formed during the reaction were adsorbed on the catalyst, and blocked 2 to 5 nm mesopores and micropores around the active component of the catalyst. These caused a decrease in specific surface area of the catalyst, further inhibiting catalytic activity.

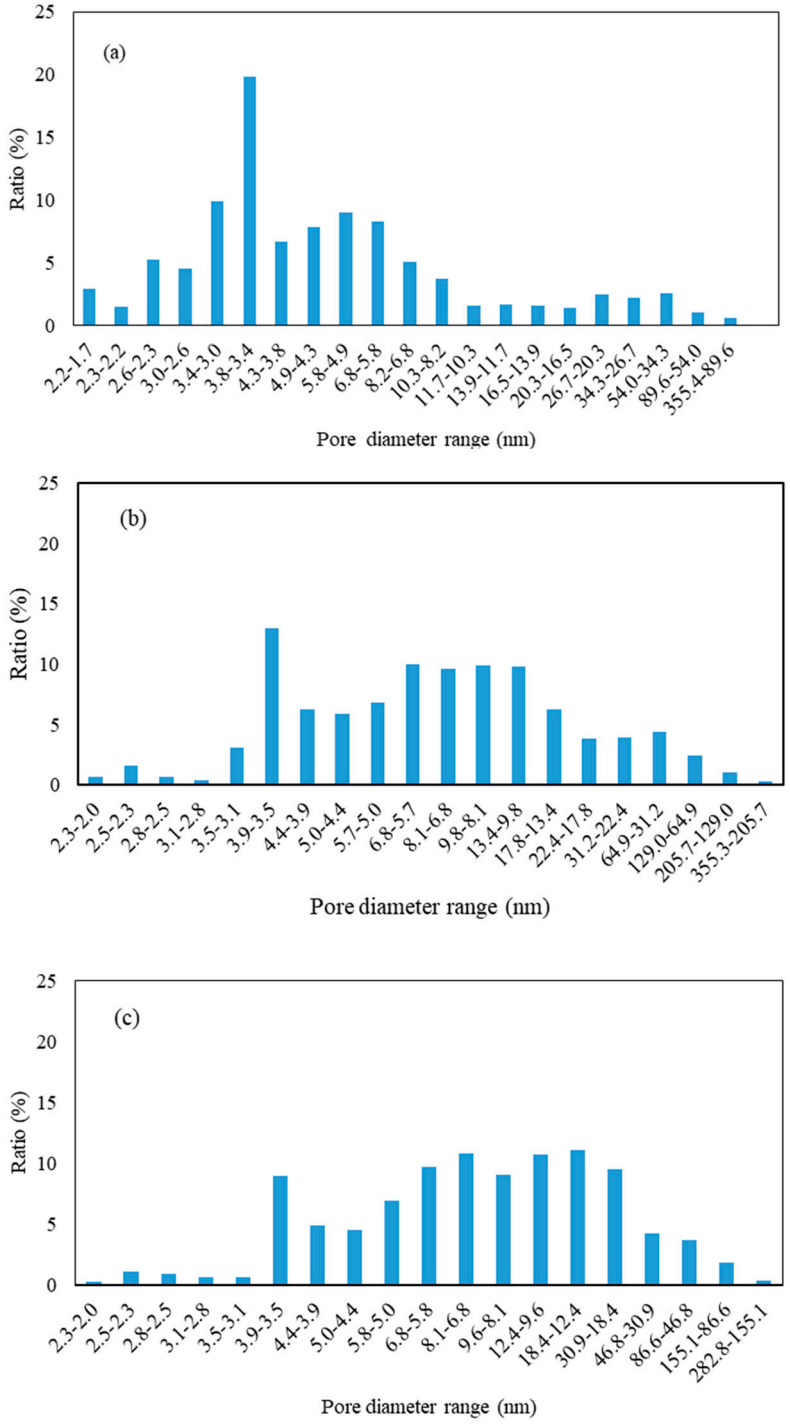

Figure 5. Pore size distribution of the fresh and poisoned catalysts. (**a**) V-0.2Ce/Ti–Zr; (**b**) S-V-0.2Ce/Ti–Zr and (**c**) HS-V-0.2Ce/Ti–Zr.

3.2.2. XRD Analysis

To further study the microstructure of the poisoned V-0.2Ce/Ti–Zr, an XRD analysis was performed. As shown in Figure 6, catalysts before and after being poisoned by SO_2 showed similar spectra. According to our previous research [12], these diffraction peaks mainly corresponded to $ZrTiO_2$, ZrO_2, V_2O_5, CeO_2 and TiO_2. Diffraction peaks of substances such as $(NH_4)_2SO_4$ or $Ce(SO_4)_2$ were not detected. The results illustrated that no sulphate with good crystal form was formed, or the amount of sulphate formed on the surface was small and highly dispersed.

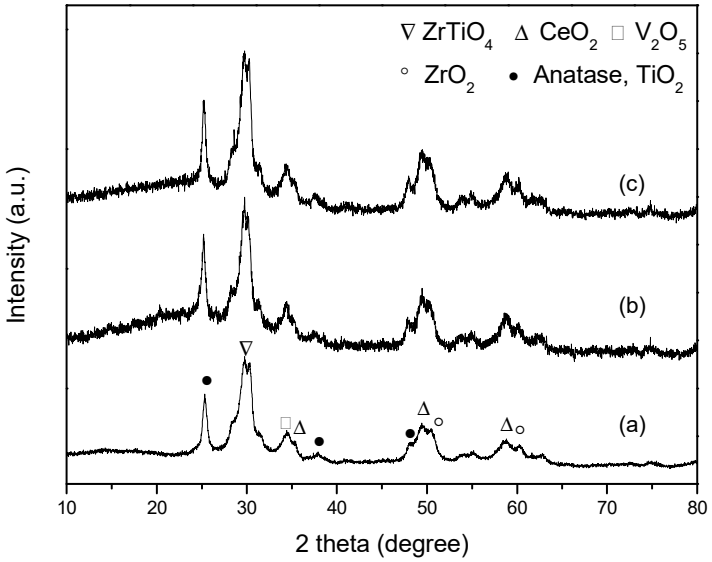

Figure 6. XRD patterns of the catalysts (**a**) V-0.2Ce/Ti–Zr, (**b**) S-V-0.2Ce/Ti–Zr and (**c**) HS-V-0.2Ce/Ti–Zr.

3.2.3. TEM and XRF Analysis

TEM was carried out to study the morphology changes of catalysts poisoned by H_2O and SO_2. As shown in Figure 7, the surface of the fresh catalyst was uniform and had a good dispersion. While for the poisoned one, it was clearly observed that the surface was covered with some substances, and the particles were agglomerate.

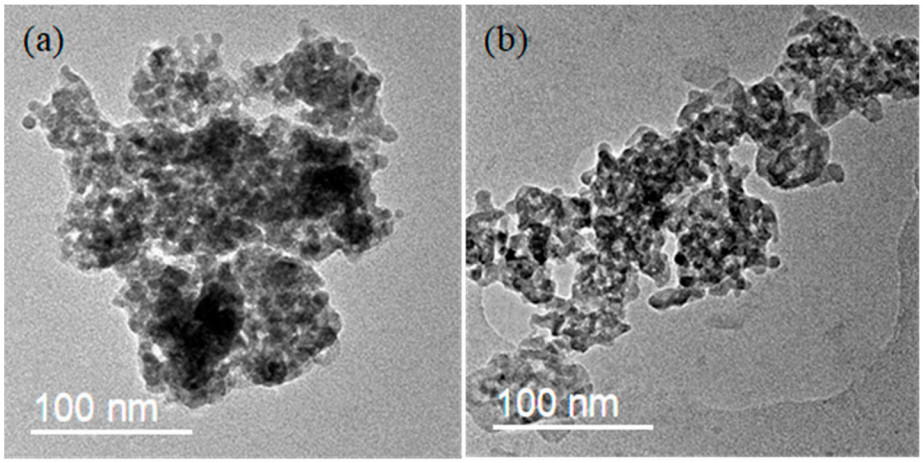

Figure 7. TEM pictures of the catalysts before and after poisoning by SO_2. (**a**) V-0.2Ce/Ti–Zr and (**b**) HS-V-0.2Ce/Ti–Zr.

Element content of the catalyst was tested and the results were shown in Table 2. No S element was detected in the S-V-0.2Ce/Ti–Zr catalyst, while a trace amount of the S element was detected in the HS-V-0.2Ce/Ti–Zr catalyst. The results revealed that when SO_2 was separately introduced, substantially no S element was present on the catalyst surface, or its content was extremely low. However, once H_2O was introduced together, SO_2 was more likely to participate in the reaction, and was present on the surface in the form of ammonium sulfate or $Ce(SO_4)_2$.

Table 2. XRF results of the catalysts before and after being poisoned by SO_2.

Sample	V	Ce	Ti	Zr	S
V-0.2Ce/Ti–Zr	0.723	12.512	1.2	34.66	0
S-V-0.2Ce/Ti–Zr	0.63	12.365	19.75	26.66	0
HS-V-0.2Ce/Ti–Zr	0.558	12.932	20.46	26.4	1.13

3.2.4. H_2-TPR Analysis

TPR profiles for catalysts before and after poisoned by SO_2 were presented in Figure 8. For the fresh catalyst, five reduction peaks were observed at 343 °C, 418 °C, 507 °C, 580 °C and 732 °C, respectively. Studies have shown that the low temperature reduction of V/TiO_2 catalyst is mainly related to the monomer vanadium or highly dispersed vanadium species [16]. Held et al. proposed that the reduction peak at about 730 °C was mainly related to V_2O_4 [17]. Based upon our previous work, peaks centered at 343 °C and 580 °C were due to the reduction of vanadium from V^{5+} to V^{4+} and V^{4+} to V^{3+}, respectively. The reduction peak centered at 418 °C was attributed to the surface (α) reduction processed of CeO_2, and the subsurface layers and deeper regions of the catalyst nanoparticles were reduced at 507 °C.

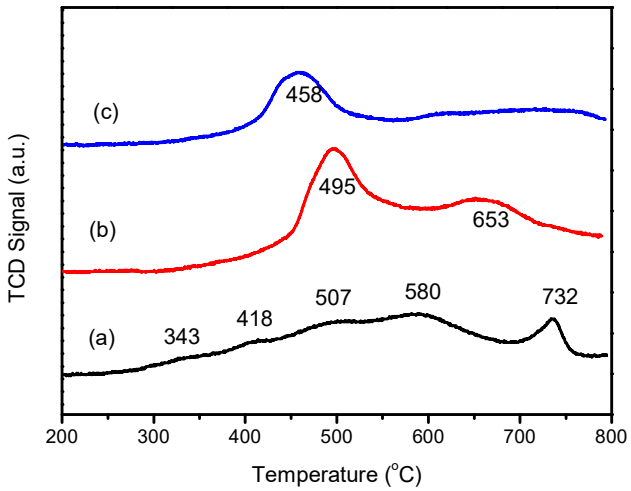

Figure 8. Hydrogen temperature-programmed desorption (H_2-TPR) patterns of the catalysts before and after being poisoned by SO_2. (**a**) V-0.2Ce/Ti–Zr, (**b**) S-V-0.2Ce/Ti–Zr and (**c**) HS-V-0.2Ce/Ti–Zr.

It could be found that the redox ability of the S-V-0.2Ce/Ti–Zr catalyst was significantly weakened, according to the fact that several peaks disappeared (343 °C, 418 °C and 580 °C). After reaction with SO_2 and H_2O, the redox ability of the HS-V-0.2Ce/Ti–Zr catalyst was further attenuated, and only one reduction peak appeared at 458 °C was detected. Peaks centered at 495 °C and 458 °C were due to the reduction of Ce^{4+}, while the peak at 653 °C was attributed to the reduction of V^{5+} to V^{3+} and the reduction of bulk phase Ce^{4+}. It could be found that the disappearance of reduction peaks related with vanadium was an important cause of catalytic deactivation. For S-V-0.2Ce/Ti–Zr sample, the α-reduction peak of Ce^{4+} disappeared, which should be related to the reduction of Ce^{4+} to Ce^{3+}. It was reported that the concentration of Ce^{3+} was used to assess the amount of oxygen formed. The oxygen vacancies were driven by the transition from Ce^{4+} to Ce^{3+}, accelerating the transport of active oxygen species and facilitating the reaction vacancies, which could explain the phenomenon that the activity of the catalyst decreased first and then gradually increased. After being poisoned by SO_2 and H_2O, the intensity of the β reduction peak (458 °C) was significantly weakened, and the reduction peak of the vanadium oxide completely disappeared. It was speculated that the formed ammonium

hydrogen sulfate was deposited on the surface of the catalyst or more stable $Ce_2(SO_4)_3$ was formed, which hindered the conversion of vanadium active species and led to a reduction of the redox ability.

3.2.5. XPS Analysis

Figure 9a showed the XPS results of Ce 3d. Peaks u‴, u″, u and v‴, v″, v can be corresponded to Ce^{4+}, while peaks u′ and v′ were assigned to Ce^{3+}, respectively. It can be seen from Figure 9a that Ce in the catalyst mainly existed in the Ce^{4+} valence state. As shown in Table 3, after reacting with 0.06% SO_2 for 2 h, the ratio of Ce^{3+}/ (Ce^{4+}+Ce^{3+}) in S-V-0.2Ce/Ti–Zr catalysts was increased to 25.15% compared with that in V-0.2Ce/Ti–Zr (24.94%), indicating more Ce^{3+} was generated. However, in the presence of SO_2 and H_2O, the ratio of Ce^{3+}/(Ce^{4+} + Ce^{3+}) was reduced again to 24.93%. Hence, it was deduced that the introduction of SO_2 promoted the conversion of Ce^{4+} and Ce^{3+}, while the formed ammonium hydrogen sulfate on the surface of the catalyst could block the path of mutual conversion between Ce^{4+} and Ce^{3+}.

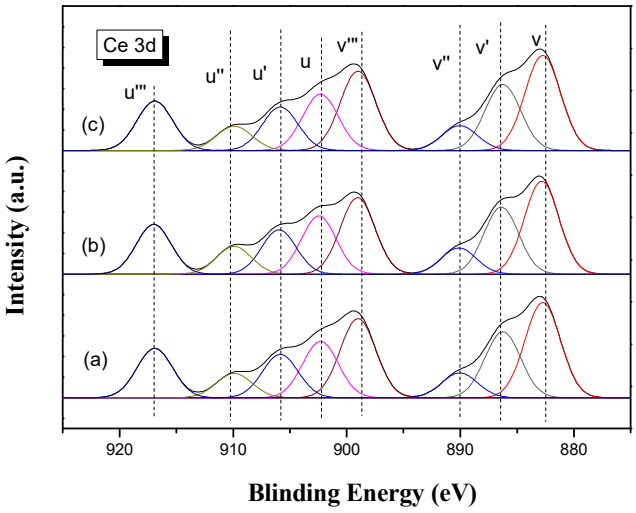

(**a**)

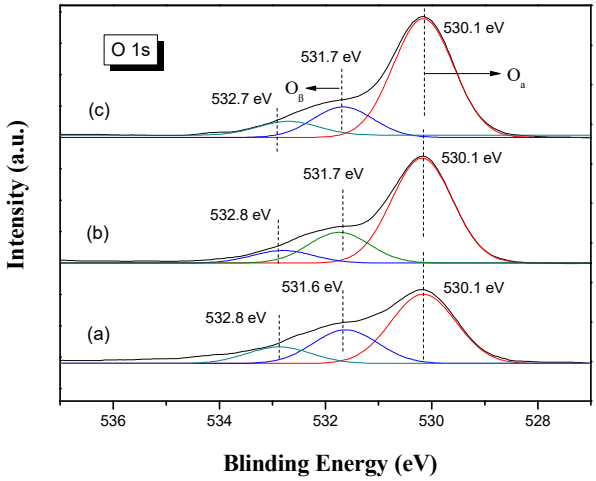

(**b**)

Figure 9. XPS spectra of Ce 3d and O 1s on catalysts before and after being poisoned by SO_2. (**a**) V-0.2Ce/Ti–Zr; (**b**) S-V-0.2Ce/Ti–Zr and (**c**) HS-V-0.2Ce/Ti–Zr.

Table 3. Peak area ratio of XPS.

Sample	Area Ratio	
	$\frac{Ce^{3+}}{Ce^{3+}+Ce^{4+}}$	$\frac{O_\beta}{O_\beta+O_\alpha}$
V-0.2Ce/Ti–Zr	24.94	28.14
S-V-0.2Ce/Ti–Zr	25.15	20.71
HS-V-0.2Ce/Ti–Zr	24.93	18.67

As shown in Figure 9b, the three peaks in O 1 s can be assigned to oxygen vacancy, adsorbed oxygen and oxygen lattice from higher binding energy to lower binding energy. The adsorbed oxygen and oxygen lattice were marked as Oβ and Oα, respectively [18,19]. The oxygen vacancy was formed due to the evolution of the oxygen lattice [20].

As can be seen in Table 3, the ratio of Oβ/(Oβ + Oα) was reduced significantly in the S-V-0.2Ce/Ti–Zr catalysts and even worse in the HS-V-0.2Ce/Ti–Zr catalysts. The existence of Oβ could promote the oxidation of NO to NO_2, which can explain the decrease in activity of the catalysts poisoned by SO_2.

3.3. In Situ DRIFTS Study

3.3.1. Sulfur Dioxide Adsorption.

Figure 10 showed the DRIFTS spectra of the V-0.2Ce/Ti–Zr catalyst in the flow of 0.06% SO_2 at 50 °C and then purged by N_2 with increasing temperatures from 50 °C to 400 °C. The peak at 1633 cm^{-1} was linked to H_2O vibration produced by the reaction of SO_2 and hydroxyl on the catalytic surface [8]. With the addition of SO_2 at 50 °C, peaks at 1376 cm^{-1}, 1338 cm^{-1}, 1265 cm^{-1}, 1097 cm^{-1} and 1049 cm^{-1} were detected. Based on the research of Peak et al. [21], the triply degenerate asymmetric stretching ν3 band were accessible to FTIR investigation, and would split into three bands when the bidentate sulfate complex was formed. Therefore, it was deduced that the bands at 1265 cm^{-1}, 1097 cm^{-1} and 1049 cm^{-1} were attributed to bidentate sulfate on V-0.2Ce/Ti–Zr. The band at 1338 cm^{-1} was assigned to the adsorbed SO_2, which mainly exists in the form of SO_3^{2-}. The band at 1376 cm^{-1} might be due to the asymmetric vibration of O = S = O covalent groups (SO_4^{2-}). When the temperature reached 100 °C, the adsorption peak at 1376 cm^{-1} disappeared [22,23].

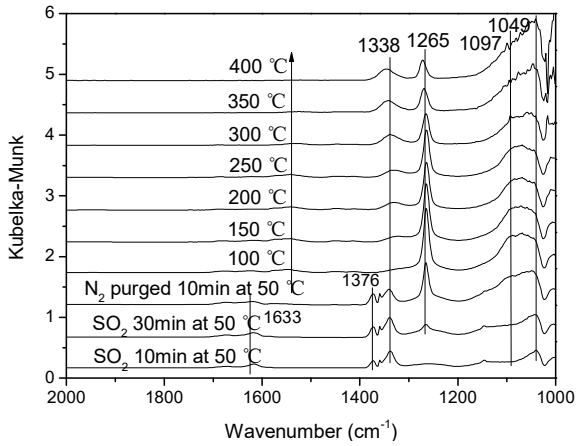

Figure 10. In situ DRIFTS spectra of V-0.2Ce/Ti–Zr treated in flowing 0.06% SO_2 at 50 °C and then purged by N_2 at a different temperature.

Figure 11a shows the in situ DRIFTS spectra of the V-0.2Ce/Ti–Zr catalyst in the flow of 0.06% SO_2 at 250 °C and then purged with N_2. After adding SO_2 for 5 min, bands at 1363 cm^{-1}, 1344 cm^{-1}, 1295 cm^{-1}, 1083 cm^{-1} and 1047 cm^{-1} were detected with increasing intensity. The bands at 1295 cm^{-1}, 1107 cm^{-1} and 1050 cm^{-1} were contributed to the bidentate sulfate on V-0.2Ce/Ti–Zr while the band at

1344 cm^{-1} was assigned to the adsorbed SO_2 (SO_3^{2-}). The band at 1363 cm^{-1} could be attributed to the asymmetric vibration of O = S = O covalent groups (SO_4^{2-}). It had been found that the O = S = O asymmetric covalent groups arose from the $VOSO_4$ adsorption peak that appeared at 1383 cm^{-1} [24,25]. Hence, we deduced the reaction between the adsorbed SO_2 with V_2O_5 in the catalyst to form the $VOSO_4$ intermediate.

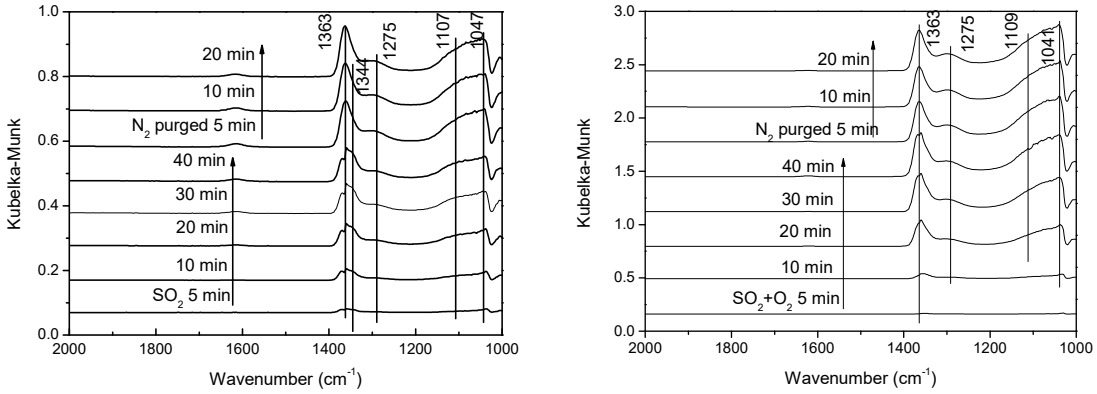

(**a**) (**b**)

Figure 11. In situ DRIFTS spectra recorded at 250 °C in a flow of 0.06% SO_2 and 0.06% SO_2 + 5% O_2 over V-0.2Ce/Ti–Zr. (**a**) SO_2 adsorption and (**b**) SO_2 + O_2 co-adsorption.

Figure 11b shows the DRIFTS spectra of the V-0.2Ce/Ti–Zr catalyst in the flow of O_2 + SO_2 at 250 °C and then purged with N_2. In general, catalysts exhibited similar peaks, while the intensity of SO_2 adsorption was enhanced significantly in the presence of O_2.

3.3.2. Effect of SO_2 on NH_3 Adsorption

Figure 12 showed the NH_3 adsorption results on V-0.2Ce/Ti–Zr in the presence of SO_2. It could be found that original adsorption capacity of NH_3 was very weak, and only the band at 1182 cm^{-1} was observed [26]. Then NH_3 was switched off and SO_2 + O_2 was introduced. The NH_3 adsorption peak was replaced by SO_4^{2-} adsorption peak quickly. Bands at 1278 cm^{-1}, 1178 cm^{-1} and 1050 cm^{-1} were assigned to SO_4^{2-} three-fold degeneracy asymmetric stretching vibration v3 and the band at 1340 cm^{-1} was assigned to the adsorbed SO_2 while the band at 1373 cm^{-1} could be attributed to the asymmetric vibration of O = S = O covalent groups (SO_4^{2-}).

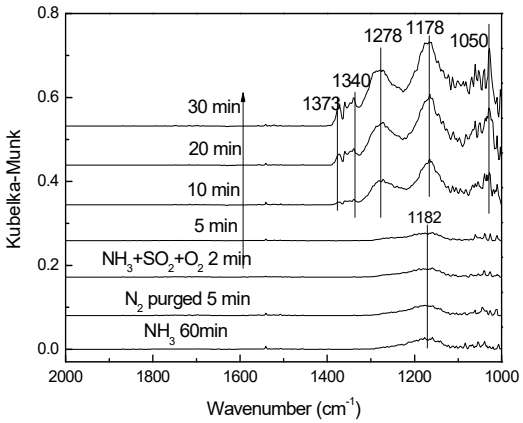

Figure 12. In situ DRIFTS spectra of V-0.2Ce/Ti–Zr pretreated by NH_3 exposed to NH_3 + SO_2 + O_2 for various times.

In Figure 13, the catalysts were pretreated by 0.06% SO_2 + O_2 for 30 min, and then exposed to 800 ppm NH_3, followed by treating with SO_2 and O_2 again. After adding NH_3, several bands at 1660 cm^{-1}, 1600 cm^{-1}, 1440 cm^{-1} and 1220 cm^{-1} were detected. The band at 1600 cm^{-1} and 1220 cm^{-1} was associated with the asymmetric and symmetric deformation vibration of NH_3 adsorbed on Lewis acid sites, while the band at 1660 cm^{-1} and 1440 cm^{-1} were due to the asymmetric and symmetric deformation of NH_4^+ bound to Brönsted acid sites [26,27]. Compared with the results of Figure 9, it could be found that the intensity of bands due to adsorbed NH_3 was significantly increased after being pretreated by SO_2 and O_2. It was deduced that the presence of SO_2 and O_2 could promote the transformation from Ce^{4+} to Ce^{3+} (the formation of $Ce_2(SO_4)_3$), resulting in the enhancement of the NH_3 adsorption ability. Furthermore, it was observed that the intensity of the NH_3 adsorption peaks did not change significantly after the introduction of SO_2 and O_2 again.

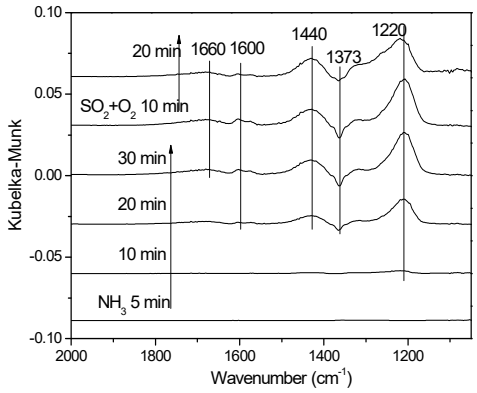

Figure 13. In situ DRIFTs spectra of V-0.2Ce/Ti–Zr pretreated by SO_2 + O_2 exposed to NH_3 for various times and then treated by SO_2 + O_2 again.

3.3.3. Effect of SO_2 on NO Adsorption

The competitive adsorption behavior of SO_2 with NO_2 in the presence of O_2 was investigated, and in situ DRIFTS results were shown in Figure 14. As shown in Figure 15, bands appeared at 1375 cm^{-1} and 1315 cm^{-1} were due to cis-$N_2O_2^{2-}$, and it could be found that the intensity of the bands increased gradually and the purge of N_2 had little influence on the adsorption bands. Band at 1190 cm^{-1} were attributed to the bridging nitrates [28]. After 10 min, SO_4^{2-} adsorption peak appeared at 1046 cm^{-1}. As the reaction went on, it divided into two adsorption peaks (1049 cm^{-1} and 1035 cm^{-1}). Along with the purge of N_2, band at 1095 cm^{-1} assigned to bidentate sulfate was observed. Furthermore, weak SO_4^{2-} adsorption band was detected at 1135 cm^{-1}.

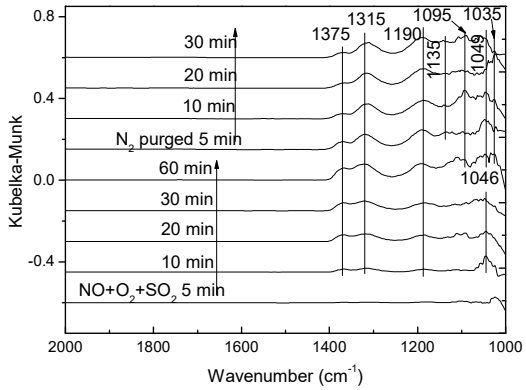

Figure 14. In situ DRIFTS spectra taken at 250 °C in a flow of 0.08% NO + 0.06% SO_2 + 5% O_2 on V-0.2Ce/Ti–Zr.

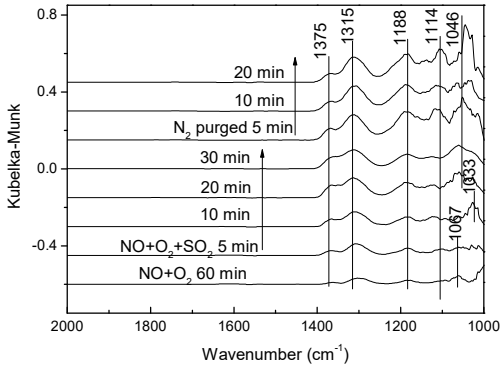

Figure 15. In situ DRIFTS spectra taken at 250 °C in a flow of 0.08% NO + 0.06% SO_2 + 5% O_2 over the NO + O_2 presorbed on V-0.2Ce/Ti–Zr.

In Figure 15, the catalyst was first treated by NO + O_2 for 60 min until the adsorption was saturated and 0.06% SO_2 was added into the cell, and then SO_2 were introduced into the in-situ cell for various times, followed by N_2 purging. As shown in Figure 15, bands due to the cis-$N_2O_2^{2-}$ were also detected at 1375 cm^{-1} and 1315 cm^{-1}. Band at 1188 cm^{-1} was assigned to the adsorbed NO_x species. Nitrate species adsorption peak appeared at 1144 cm^{-1} and 1067 cm^{-1} after NO + O_2 pre-adsorption. Once feeding SO_2, the intensity of the bands at 1375 cm^{-1}, 1315 cm^{-1}, 1188 cm^{-1} and 1144 cm^{-1} were strengthened and the purge of N_2 had little influence on the adsorption bands, while the band at 1067 cm^{-1} gradually disappeared. The SO_4^{2-} adsorption peak appeared at 1046 cm^{-1}.

Based on the analysis above, it could be concluded that the presence of SO_2 could promote NO adsorption on the catalyst surface. In addition, our previous research has a certified catalyst that mainly follows the Eley–Rideal (E-R) mechanism, and NO adsorption on the catalyst surface restrains the SCR reaction [12]. Thus, it can explain the decrease of catalyst activity when SO_2 was injected.

3.3.4. Effect of SO_2 on NH_3 + NO + O_2 Co-Adsorption

As shown in Figure 16, in the presence of NH_3 + NO + O_2, only the band at 1205 cm^{-1} due to adsorbed NH_3 was observed. After 0.06% SO_2 was injected, adsorption intensity of bands due to adsorbed NH_3 decreased rapidly. These results indicated that the presence of SO_2 significantly weakened the NH_3 adsorption, which was consistent with the result of Figure 12. After the introduction of SO_2 for 20 min, bands at 1373 cm^{-1}, 1280 cm^{-1}, 1095 cm^{-1} and 1043 cm^{-1} were detected. The band at 1373 cm^{-1} could be attributed to the asymmetric vibration of O = S = O covalent groups and bands at 1280 cm^{-1}, 1095 cm^{-1} and 1043 cm^{-1} were assigned to SO_4^{2-} three-fold degeneracy asymmetric stretching vibration v3. In our previous study [12], the SCR reaction over V-0.2Ce/Ti–Zr obeyed the E-R mechanism. Hence, as an important reaction substance, the weakening of NH_3 adsorption would greatly inhibit the SCR reaction.

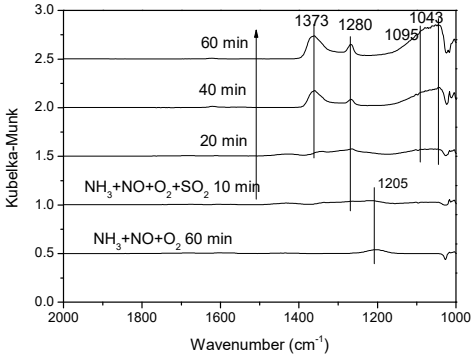

Figure 16. In situ DRIFTS spectra of the NH_3 + NO + O_2 reaction on V-0.2Ce/Ti–Zr (250 °C) with 0.06% SO_2.

3.4. Possible SO_2 Reaction Mechanism Over The Catalyst

The adsorption ability of SO_2 had something with its concentration. There was no adsorption when SO_2 concentration was low, which explained the stable activity of catalysts at low SO_2 concentration. With the increase of the SO_2 concentration, SO_2 and SO_4^{2-} adsorption appeared. SO_2 was adsorbed on the surface in the form of SO_3^{2-}. The consumption of surface OH species meant that SO_2 was able to react with surface hydroxyl groups to form adsorbed H_2O. It was speculated that in the presence of O_2, SO_2 would react with NH_3 to form $(NH_4)_2SO_4$, which could deposit on the surface of the catalyst and reduce the catalyst activity. The sulfate products could combine with Ce to form more stable $Ce(SO_4)_2$. The reaction might be proposed as follows:

$$SO_2(g) + O^{2-}(a) \rightarrow SO_3^{2-}(a), \quad (1)$$

$$SO_2(g) + 2OH^-(a) \rightarrow SO_3^{2-}(a) + H_2O, \quad (2)$$

$$O_2(g) \rightarrow 2[O](a), \quad (3)$$

$$SO_3^{2-}(a) + [O](a) \rightarrow SO_4^{2-}(a) \quad (4)$$

$$SO_4^{2-}(a) + 2NH_4^+(a) \rightarrow (NH_4)_2SO_4 \quad (5)$$

$$Ce^{4+} + SO_4^{2-} \rightarrow Ce(SO_4)_2 \quad (6)$$

According to the in-situ DRIFTS results and other study [19], $SO_2(SO_3^{2-})$ could react with V^{5+}–OH to form $VOSO_4$ intermediate.

$$SO_3^{2-}(a) + V^{5+}\text{-}OH(a) \rightarrow VOSO_4 \quad (7)$$

With the time passing, absorbed SO_2 (SO_3^{2-}) contacted with the active component Ce and caused the transformation from Ce^{4+} to Ce^{3+}, increasing the oxygen vacancy and enhancing the NH_3 adsorption ability, which can explain the recovery of activity. The presence of O_2 promoted the redox of SO_2 and formation of sulfate $Ce_2(SO_4)_3$.

$$3SO_2 + 2CeO_2 + O_2 \rightarrow Ce_2(SO_4)_3 \quad (8)$$

4. Conclusions

Catalyst activity test results showed that low concentration SO_2 (<0.02%) had little influence on catalyst activity. With increasing SO_2 concentration, NO_x conversion of the catalyst gradually decreased but could restore to the original level when stopping feeding SO_2. A reversible deactivation would occur in the presence of H_2O. However, in the presence of SO_2 and H_2O, the catalyst was irreversibly deactivated, which was worse than that of adding SO_2 or H_2O alone.

The characterization results showed that the BET specific surface area of the catalysts poisoned by SO_2 were reduced, and the redox capacity were significantly weakened. The sulfuration of the active component Ce and the deposition of ammonium sulfate might be the causes of the deactivation. XPS analysis showed that the presence of SO_2 promoted the generation of Ce^{3+}, which probably promoted the SCR reaction.

In situ DRIFTS analysis indicated that the adsorption capacity of SO_2 was enhanced in the presence of O_2. The presence of SO_2 would inhibit the adsorption of NH_3. At the same time, the NO adsorption ability of the catalyst was enhanced to some extent by SO_2. Moreover, the NH_3 adsorption ability of the catalyst with pre-adsorption of $SO_2 + O_2$ was markedly enhanced, indicating that when $SO_2 + O_2$ existed, more Ce^{3+} and oxygen vacancy were produced. These conclusions might contribute to a better understanding of the SO_2 poisoning mechanism over the V_2O_5–CeO_2/TiO_2–ZrO_2 catalyst.

Author Contributions: Formal analysis, P.W.; S.W. and W.G.; Investigation, Y.Z.; Methodology, K.Z. and K.S.; Supervision, K.S.; Writing-original draft, Y.Z.

Acknowledgments: This work was supported by the Key Research and Development Projects of Jiangsu Province (BE2017716), National Key R&D Program of China (2017YFB0603201) and Environmental nonprofit industry research subject (2016YFC0208102).

Conflicts of Interest: The authors declare no conflict of interest.

References

1. Fan, Y.Z.; Cao, F.H. Thermal decomposition kinetics of ammonium sulfate. *J. Chem. Eng. Chin. Univ.* **2011**, *25*, 341–346.
2. Zhang, W.; Chen, H.; Xia, Y. Effects of Nd-modification on the activity and SO_2 resistance of MnO_x/TiO_2 catalyst for low-temperature NH_3-SCR. *New J. Chem.* **2018**, *42*, 12845–12852.
3. Qi, G.; Yang, R.T. Low-temperature selective catalytic reduction of NO with NH_3 over iron and manganese oxides supported on titania. *Appli. Catal. B: Environ.* **2003**, *44*, 217–225. [CrossRef]
4. Wei, L.; Cui, S.; Guo, H. *Mechanism of SO_2 Influence on Mn/TiO_2 for Low Temperature SCR Reaction*; Han, Y., Ed.; Chinese Materials Conference; Springer: Berlin, Germany, 2017; pp. 789–796.
5. Jiang, B.Q.; Wu, Z.B.; Liu, Y. DRIFT study of the SO_2 effect on low-temperature SCR reaction over Fe-Mn/TiO_2. *J Phys Chem. C* **2010**, *114*, 4961–4965. [CrossRef]
6. Liu, F.; He, H. Selective catalytic reduction of NO with NH_3 over manganese substituted iron titanate catalyst: Reaction mechanism and H_2O/SO_2 inhibition mechanism study. *Catal. Today.* **2010**, *153*, 70–76. [CrossRef]
7. Pan, S.; Luo, H.; Li, L. H_2O and SO_2 deactivation mechanism of MnO_x/MWCNTs for low-temperature SCR of NO_x with NH_3. *J. Mol. Catal. A: Chem.* **2013**, *377*, 154–161. [CrossRef]
8. Gu, T.; Liu, Y.; Weng, X. The enhanced performance of ceria with surface sulfation for selective catalytic reduction of NO by NH_3. *Catal. Commun.* **2010**, *12*, 310–313. [CrossRef]
9. Xu, Q.; Yang, W.; Cui, S. Sulfur resistance of Ce-Mn/TiO2 catalysts for low-temperature NH_3–SCR. *R. Soc. Open Sci.* **2018**, *5*, 171846. [CrossRef]
10. Yamaguchi, T. Recent progress in solid superacid. *Cheminform* **1990**, *61*, 1–25. [CrossRef]
11. Kwon, D.W.; Nam, K.B.; Hong, S.C. The role of ceria on the activity and SO_2 resistance of catalysts for the selective catalytic reduction of NO_x by NH_3. *Appli. Catal. B Environ.* **2015**, *166–167*, 37–44. [CrossRef]
12. Zhang, Y.; Guo, W.; Wang, L. Characterization and activity of V_2O_5-CeO_2/TiO_2-ZrO_2 catalysts for NH_3-selective catalytic reduction of NO*x*. *Chin. J. Catal.* **2015**, *36*, 1701–1710. [CrossRef]
13. Zhang, Y.; Zhu, X.; Shen, K. Influence of ceria modification on the properties of TiO_2-ZrO_2 supported V_2O_5 catalysts for selective catalytic reduction of NO by NH_3. *J. Colloid Interface Sci.* **2012**, *376*, 233–238. [CrossRef] [PubMed]
14. Zhang, Y.; Yue, X.; Huang, T. In Situ DRIFTS Studies of NH_3-SCR Mechanism over V_2O_5-CeO_2/TiO_2-ZrO_2 Catalysts for Selective Catalytic Reduction of NO_x. *Materials* **2018**, *11*, 1307. [CrossRef] [PubMed]
15. Xu, W.; He, H.; Yu, Y. Deactivation of a Ce/TiO_2 Catalyst by SO_2 in the Selective Catalytic Reduction of NO by NH_3. *J. Phys. Chem. C* **2009**, *113*, 4426–4432. [CrossRef]
16. Pena, M.L.; Dejoz, A.; Fornes, V. V-containing MCM-41 and MCM-48 catalysts for the selective oxidation of propane in gas phase. *Appli. Catal. A Gen.* **2001**, *209*, 155–164. [CrossRef]
17. Held, A.; Kowalska-Kuś, J.; Nowińska, K. Epoxidation of propene on vanadium species supported on silica supports of different structure. *Catal. Commun.* **2012**, *17*, 108–113. [CrossRef]
18. Jiang, H.; Wang, C.; Wang, H. Synthesis of highly efficient MnO_x catalyst for Low-Temperature NH_3-SCR prepared from Mn-MOF-74 template. *Mater. Lett.* **2016**, *168*, 17–19. [CrossRef]
19. Liu, J.; Guo, R.; Li, M. Enhancement of the SO_2 resistance of Mn/TiO_2 SCR catalyst by Eu modification: A mechanism study. *Fuel* **2018**, *223*, 385–393. [CrossRef]
20. Zhang, L.; Zhang, D.; Zhang, J. Design of meso-TiO_2@MnO_x-CeO_x/CNTs with a core-shell structure as $DeNO_x$ catalysts: Promotion of activity, stability and SO_2-tolerance. *Nanoscale* **2013**, *5*, 9821. [CrossRef] [PubMed]
21. Peak, D.; Ford, R.G.; Sparks, D.L. An in situ ATR-FTIR investigation of sulfate bonding mechanisms on goethite. *J. Colloid Inter. Sci.* **1999**, *218*, 289–299. [CrossRef] [PubMed]
22. Luo, T.; Gorte, R.J. Characterization of SO_2-poisoned ceria-zirconia mixed oxides. *Appli. Catal. B Environ.* **2004**, *53*, 77–85. [CrossRef]

23. Yamaguchi, T.; Jin, T.; Tanabe, K. Structure of acid sites on sulfur-promoted iron oxide. *J. Phys. Chem.* **1986**, *90*, 3148–3152. [CrossRef]
24. Zhang, L.; Li, L.L.; Cao, Y.; Yao, X.J.; Ge, C.Y.; Gao, F.; Yu, D.; Tang, C.J.; Dong, L. Getting insight into the influence of SO_2 on TiO_2/CeO_2 for the selective catalytic reduction of NO by NH_3. *Appli. Cataly. B Environ.* **2015**, *165*, 589–598. [CrossRef]
25. Liu, Y.; Shu, H.; Xu, Q. FT-IR study of the catalytic oxidation of SO_2 during the process of selective catalytic reduction of NO with NH_3 over commercial catalysts. *J. Fuel Chem. Technol.* **2015**, *43*, 1018–1024. [CrossRef]
26. Zhang, Q.; Fan, J.; Ning, P. In situ DRIFTS investigation of NH_3-SCR reaction over CeO_2 /zirconium phosphate catalyst. *Appli. Surf. Sci.* **2018**, *435*, 1037–1045. [CrossRef]
27. Gelves, J.F.; Dorkis, L.; Márquez, M.A. Activity of an iron Colombian natural zeolite as potential geo-catalyst for NH_3-SCR of NO_x. *Cataly. Today* **2019**, *320*, 112–122. [CrossRef]
28. Jin, C.M.; Xin, Y.L.; Wen, B.S. Enhancement of low-temperature catalytic activity over highly dispersed Fe-Mn/Ti Catalyst for selective catalytic reduction of NO_x with NH_3. *Ind. Eng. Chem. Res.* **2018**, *57*, 10159–10169.